Stability and Metastability of Liquid water in a Machine-learned Coarse-grained Model with Short-range Interactions

Debdas Dhabal,[a] Subramanian K. R. S. Sankaranarayanan,[b,c] and Valeria Molinero[a,*]

[a]Department of Chemistry, The University of Utah, Salt Lake City, Utah 84112-0850, United States

[b]Department of Mechanical and Industrial Engineering, University of Illinois, Chicago, Illinois 60607, United States.

[c]Center for Nanoscale Materials, Argonne National Laboratory, Lemont, Illinois 60439, United States.

ABSTRACT. Coarse-grained water models are ~100 times more efficient than all-atom models, enabling simulations of supercooled water and crystallization. The machine-learned monatomic model ML-BOP reproduces the experimental equation of state (EOS) and ice-liquid thermodynamics at 0.1 MPa on par with all-atom TIP4P/2005 and TIP4P/Ice. These all-atom models were parameterized using high-pressure experimental data, and are either accurate for water's EOS (TIP4P/2005) or ice-liquid equilibrium (TIP4P/Ice). ML-BOP was parameterized from temperature-dependent ice and liquid experimental densities and melting data at 0.1 MPa; its only pressure training is from compression of TIP4P/2005 ice at 0 K. Here we investigate whether ML-BOP replicates the experimental EOS and ice-water thermodynamics along all pressures of ice I. We find that ML-BOP reproduce the temperature, enthalpy, entropy and volume of melting of hexagonal ice up to 400 MPa and the EOS of water along the melting line with accuracy that rivals both TIP4P/2005 and TIP4P/Ice. We interpret that the accuracy of ML-BOP originates from its ability to capture the shift between compact and open local structures to changes in pressure and temperature. ML-BOP reproduces the sharpening of the tetrahedral peak of the pair distribution function of water upon supercooling, and its pressure dependence. We characterize the region of metastability of liquid ML-BOP with respect to crystallization and cavitation. The accessibility of ice crystallization to simulations of ML-BOP, together with its accurate representation of the thermodynamics of water, makes it promising for investigating the interplay between anomalies, glass transition, and crystallization under conditions challenging to access through experiments.

1. INTRODUCTION

A multitude of water models have been developed since the first one by Bernal and Fowler in 1933.[1] These models have been used to investigate the structure, transport, anomalies, and the limits of stability and metastability of liquid water in the pressure-temperature space.[2-19] The anomalies of water have been interpreted to arise from the two-state thermodynamics of the liquid, which can be construed as a mixture of four-coordinated and higher coordination local order motifs with proportions that depend on temperature and pressure.[20-22] Consistent with these models, molecular simulations indicate that the fraction of four-coordinated water molecules increases upon supercooling and decreases on compression.[20, 23-25] The height g_2 of the second peak of the oxygen-oxygen radial distribution function provides another, average measure of tetrahedrality that can be computed from both experiments and simulations.[26] The temperature dependence of the experimental g_2 at 1 bar is well reproduced by the all-atom flexible polarizable MB-Pol[27] and iAMOEBA[28] models, as well as the all-atom rigid non-polarizable TIP4P/2005[27, 28] model. However, not all water models in these classes reproduce the temperature dependence of g_2.[27, 28] To our knowledge, the pressure dependence of this quantity has not been reported for any water model.

In the last years there has been a growing interest in developing computationally very efficient coarse-grained (CG) water models with resolution ranging from one to four molecules per coarse-grained particle.[11, 13, 15, 29-37] On the coarser end, the MARTINI model maps four water molecules into a single bead.[29] This low resolution results in poor representation of water compressibility and surface tension, and inability to stabilize ice I. Single molecule resolution CG models of water based on isotropic two-body potentials have been developed using relative entropy minimization (REM), structure matching, and force matching procedures.[30, 31, 34, 38] While many of these CG models reproduce the pair structure of water and the existence of a density anomaly,[30, 31] isotropic models are unable to simultaneously represent the energetics and pair distribution function of water,[30] and transferability can only be achieved if their force field parameters are state point dependent.[30, 34, 39] The monatomic water model mW[11] was the first to address that limitation through a combination of two and three-body short-range potentials that encourage tetrahedral local order in water. mW is a reparameterization of the Stillinger-Weber (SW) silicon potential,[40] and is built on the premise that the thermodynamics of water does not stem from the specific nature of the hydrogen bonding interactions but from the tetrahedral-like order it encourages in the liquid.[11] mW produces the characteristic anomalies and polyamorphism of water,[11, 23, 41-45] and was the first water model to spontaneously nucleate and grow ice I from supercooled water[45-48] (a pioneering simulation with a modified TIP4P model previously nucleated a different hypothetical ice polymorph.[49]). However, the tetrahedrality of mW increases more weakly than that of water upon supercooling[20, 28, 50] and diminishes less upon compression.[11] It is still an open question whether other CG models based on short-

ranged interactions can reproduce the temperature and pressure dependence of the structure of liquid water.

Reproducing thermodynamic properties such as the ice-liquid phase diagram remains a stringent test for water models.[3] The melting temperature T_m of a water model was first calculated by molecular simulations in 2004, when Abascal and Vega computed the T_m of TIP4P and SPC/E at 1 bar.[51] The many-body all-atom polarizable MB-Pol model[17, 52, 53] predicts T_m = 263.5 K at 0.1 MPa,[8] 3.5% below the 273.15 K of water. TIP4P/Ice and TIP4P/2005 models are considered the most accurate among rigid non-polarizable water models.[2, 3] TIP4P/Ice reproduces the pressure dependence of the melting point of ice Ih within 2% of the experimental value.[3] TIP4P/2005 systematically underestimates the ice Ih-water melting temperature by about 8%, although it reproduces well the anomalies and properties of liquid water.[2, 54] These results suggest that the accuracy in reproducing the ice-liquid equilibrium line is not intrinsically correlated to the level of detail of the water model.

It has been shown that mW accurately reproduces ice Ih melting temperature at atmospheric pressure,[55] but it severely underestimates the slope of the melting line[56] because mW overestimates the density of ice and its liquid phase is less compressible than water.[11, 56] Additional CG water models based on the SW form have been developed using relative entropy minimization (mX^{REM}, where X = TIP3P, SPC/E, TIP4P-Ew, and TIP4P/2005),[33] uncertainty quantification (mW_{UQ}),[32] and genetic algorithms (ML-mW).[13] While these SW water models also present water-like anomalies and crystallize to ice Ih, none can reproduce both the melting temperature of water at 0.1 MPa and its pressure dependence.[13, 32, 33, 56] It is not yet known whether CG models can attain the level of accuracy of all-atom models in the predictions of the phase behavior of water.

Very recently, Chan *et al.* developed the machine learned bond-order potential (ML-BOP) monatomic water model.[13] Same as mW, ML-BOP is based on the functional form of a short-ranged silicon model. The functional form of ML-BOP is the Tersoff potential[57] (see Section 2.1), which differs from the SW form in multiple ways. First, SW is a sum of two-body attractive and three-body repulsive interactions, where the three-body term has an angular dependence that penalizes non-tetrahedral angles among the water sites. On the other hand, the forces in Tersoff are pairwise, but the attractive term is modified by an embedded bond-order parameter that depends on the three-body angles formed by the atoms in the pair with their close neighbors. Second, the angular potential in SW is a simple cosine quadratic function, whereas in Tersoff the cosine quadratic form is embedded in a more complex function with two more parameters that provide flexibility on the relative penalties to higher and lower angles. Third, Tersoff allows for the independent modulation of the steepness and cutoff of the pairwise interaction terms, while there is a single cutoff in SW. Chan *et al.* have demonstrated that the control of the steepness and cutoff are key for the performance of the ML-BOP model.[13]

The parameters of ML-BOP were optimized with a machine-learning workflow using experimental data of water at 0.1 MPa: densities of ice from 273 to 213 K, densities of liquid water from 338 to 253 K, and the temperature and enthalpy of melting of ice I. These two melting properties set the energy scale of the model. That experimental data set was complemented with the equation of state $p(V)$ for TIP4P/2005 ice Ih at 0 K (i.e. energy minimized) sampling volumes from -3% to 3% of the equilibrium one at 0.1 MPa;[13] this is the only pressure dependence considered in the parameterization. It should be noted that structural data of liquid water or ice were not part of the training data in the development of ML-BOP.

The use of only thermodynamic, and not structural, properties in the parameterization of ML-BOP,[13] resembles the strategy used for the parameterization of mW.[11] The latter, however, matched only the experimental density and enthalpy of vaporization of water at 298 K and the melting temperature of ice –all at 0.1 MPa- and used a simple non-iterative procedure to determine the size and energy scales, and the weight of the three-body interaction from these three data points,[11] leaving the 6 other parameters as in SW silicon.[40] Chan et al. used not only an expanded training set that included both liquid and ice densities in a wide range of temperatures, but also performed an extensive optimization of all 11 parameters of the Tersoff model using the hierarchical objective genetic algorithm, (HOGA), a multilevel evolutionary strategy.[13]

ML-BOP is comparable to mW in terms of computational efficiency, but it outperforms mW across several metrics.[13] Moreover, ML-BOP has been shown to reproduce the liquid-ice I equilibrium thermodynamics at 0.1 MPa with same or higher accuracy than the best all-atom models.[13] Remarkably, ML-BOP reproduces the equation of state $\rho(T,p)$ of water at 0.1 MPa with accuracy comparable to TIP4P/2005,[13] and better than TIP4P/Ice and MB-Pol.[13, 58] The ability of ML-BOP to reproduce the equation of state $\rho(T,p)$ of water across a wide range of pressures has not yet been investigated. Our first aim in this study is to address whether ML-BOP can reproduce structural, thermodynamics and crystallization properties of water across the range of pressures of stability of ice I.

A phase transition between two metastable liquids has been reported for several models of water,[59-61] and proposed to explain the anomalies of its liquid phase.[18, 59, 62] The unavoidable crystallization of ice at conditions where this liquid-liquid phase transition (LLPT) is predicted to occur hampers its conclusive identification in experiments[26, 62, 63] and poses fundamental questions about the interplay between crystallization and polyamorphic transformation in supercooled water.[45] Likewise, cavitation of stretched water hinders the quest to characterize the anomalies of super-

cooled water at negative pressures -the double metastable regime- argued to hold clues on the existence and thermodynamic origin of the putative liquid-liquid transition and anomalies of water.[22, 64-66] Determining the stability of metastable liquid water with respect to crystallization and cavitation is a first step towards identifying the origin of the anomalies in water. Our second aim in this study is to demarcate the kinetic limits of metastability of liquid ML-BOP upon extension and supercooling, towards a future characterization of the anomalies and investigation of the existence of a liquid-liquid transition in this model.

2. METHODS

2.1. ML-BOP Water Model

The ML-BOP model developed by Chan *et al.*[13] is a parameterization of the Tersoff potential:[57]

$$V_{ij} = f_C(r_{ij})\left[f_R(r_{ij}) + b_{ij} f_A(r_{ij})\right], \qquad (1)$$

where, r_{ij} is the distance between particles *i* and j, $f_C(r_{ij})$ is a smooth cutoff function represented as:

$$f_C(r_{ij}) = \begin{cases} 1, & r_{ij} < R - D \\ \frac{1}{2} - \frac{1}{2}\sin\left(\frac{\pi(r_{ij} - R)}{2D}\right), & R - D < r_{ij} < R + D \\ 0, & r_{ij} > R + D \end{cases} \qquad (2)$$

with R = 3.282761 Å and D = 0.270511 Å, and $f_R(r_{ij})$ and $f_A(r_{ij})$ are, respectively, repulsive and attractive pair potentials:

$$f_R(r_{ij}) = Ae^{-\lambda_1 r_{ij}} \qquad (3)$$

$$f_A(r_{ij}) = -Be^{-\lambda_2 r_{ij}} \qquad (4)$$

where A = 38841.54554 kcal mol^{-1} and B = 10922.14676 kcal mol^{-1} are the energy scale parameter and λ_1 = 2.750522 Å^{-1} and $\lambda_2 = 2.199640$ Å^{-1} are the length-scale parameters for the two-body interactions. b_{ij} in eqn. 1 is the bond-order parameter that scales the attractive pair interaction according to the angles of the pair with neighboring water molecules:

$$b_{ij} = \left(1 + \beta^n \xi_{ij}^n\right)^{-\frac{1}{2n}}, \qquad (5)$$

where n = 0.770018, $\beta = 10^{-6}$ and

$$\xi_{ij} = \sum_{k \neq i,j} f_C(r_{ik}) g(\theta_{ijk}) \exp\left[\lambda_3^m (r_{ij} - r_{ik})^m\right], \qquad (6)$$

where m = 1, $\lambda_3 = 0.0$ making $\exp\left[\lambda_3^m (r_{ij} - r_{ik})^m\right] = 1$, and $g(\theta_{ijk})$ is a function of the angle between particles *i*, *j* and *k*,

$$g(\theta) = \gamma_{ijk}\left(1 + \frac{c^2}{d^2} - \frac{c^2}{[d^2 + (\cos\theta - \cos\theta_0)^2]}\right), \qquad (7)$$

where the weight $\gamma_{ijk} = 1.0$ and the minimum of $g(\theta_{ijk})$ occurs at $\cos\theta_0 = -0.471029$, that corresponds to an angle of 118°. The parameters c = 77638.534354 and d = 16.148387 control the strength and sharpness of the angular form, respectively.

2.2. Molecular Dynamics Simulations

2.2.1. Simulation setting.

All the simulations presented in the manuscript are performed using the LAMMPS[67] package. We perform simulations with the coarse-grained (CG) models ML-BOP,[13] ML-mW,[13] and mW[11] and the all-atom (AA) TIP4P/2005 model. [2] The equations of motions are integrated using the velocity-Verlet algorithm with a timestep of 5 fs for the coarse-grained water (CG) models and 1 fs for the AA model. All simulations are periodic in the three Cartesian directions and evolved in the *NpT* ensemble, controlling both the temperature and pressure through the Nose-Hoover thermostat and barostat. The time constant for thermostat and barostat are 0.5 and 5 ps respectively for all CG water models. For TIP4P/2005 model, the thermostat and barostat constants during the equilibration simulations are 0.1 ps and 1 ps respectively, whereas, during the production simulations these are 1 ps and 10 ps respectively.

The bonds and angles in the all-atom water molecules are constrained using the SHAKE algorithm.[68] The short-range electrostatic and Lennard-Jones interactions are calculated within a cutoff distance of 12 and 10 Å, respectively. The particle-particle particle-mesh (PPPM) solver[69] is used to compute the long-range electrostatic interactions.

The initial configurations for all the liquid simulation boxes are generated using the Packmol software package.[70] The ice Ih configurations are generated using the GenIce package.[71] The simulation snapshots presented in the manuscript are prepared using Visual Molecular Dynamics software VMD.[72] Additional details of calculations of properties discussed in the manuscript are included below.

2.2.2. Structural properties.

We calculate three structural properties of water: radial distribution function, structure factor, and angular distribution function. For the calculation of these properties for liquid ML-BOP,[13] mW[11] and ML-mW,[13] we first prepare an initial configuration containing 8000 water beads randomly generated in a cubic simulation box using the Packmol package.[70] This randomly generated water box is first energy minimized and then equilibrated for 5 ns in the NPT ensemble at 298 K and 0.1, 100, 200, 300, and 362 MPa, and at 248 K and 0.1 MPa and 362 MPa. We also perform simulations at 0.1 MPa at temperatures ranging from 318 to 215 K. For each thermodynamic state we perform a 40 ns production run saving coordinates every 50 ps. TIP4P/2005 simulation cells also contain 8000 water molecules. The cubic simulation box is equilibrated for 2 ns at 298 K at pressures 0.1, 100.4, 202, 301.8, and 36 2 MPa, and at 0.1 MPa at temperatures 248, 268, 298, 318, and 358 K. At each thermodynamic

state we perform 4 ns production simulations, collecting configurations every 5 ps.

These simulations are used for the structural analysis presented in Section 3.1. The radial distribution function (RDF), $g_{OO}(r)$, and structure factors $S_{OO}(q)$ are calculated using an in-house code. We calculate the structure factor by Fourier transforming the corresponding radial distribution function as:[24, 73]

$$S_{OO}(q) = 1 + 4\pi\rho \int_0^\infty (g_{OO}(r) - 1)\frac{\sin qr}{q} r\mathrm{d}r \quad (8),$$

where $g_{OO}(r)$ is the oxygen-oxygen radial distribution function, ρ is the number density of the liquid and q is the wave number.

We calculate the O-O-O angular distribution function, $P(\theta)$, at the aforementioned temperatures and pressures as in ref. [24], using as cutoff the minimum of the pair distribution function, 3.35 Å, for ML-BOP and TIP4P/2005. We calculate the RDF and ADF for mW at 298 K and 0.1, 100, 202, 301.8, and 362 MPa pressure and for ML-mW at 298 K and 0.1, 100.4, 202, 301.8, and 362 MPa following the same protocols as for ML-BOP. The cutoff distance for ADF calculation of mW and ML-mW is the first minimum in their RDF, 3.5 and 3.7 Å, respectively.

2.2.3. Melting temperature.

To calculate the melting temperature of ice Ih as a function of pressure for the ML-BOP model, we first generate a rectangular ice slab with dimensions ~46.5 Å × 53 Å × 113.6 Å containing 9216 water molecules using the GenIce package.[71] We then remove all hydrogens to treat oxygen atoms as a coarse-grained water bead in the system and minimize the energy at -100 MPa to 400 MPa with anisotropic coupling in the three dimensions using the *box/relax* command in LAMMPS. The minimized ice slab is equilibrated at a temperature 20 K below the experimental melting temperature at each pressure. We then melt half of the simulation box keeping the other half frozen to prepare systems with coexisting solid-liquid phases. Supp. Info. Figure S1a shows the initial simulation setup with the coexisting phases at 0.1 MPa. At each pressure, we perform NPT simulations at different temperatures near the expected T_m and follow whether the ice grows (and energy decreases) or melts (and energy increases) within 50 ns. Supp. Info. Figure S1b and c show the final simulation box at varying temperatures and 0.1 MPa pressure, and how the potential energy of the system changes throughout the 50 ns simulation. We determine the melting temperature, T_m as the mean between the highest temperature at which the amount of ice decreases and the lowest temperature at which the amount of ice increases in the simulations at each pressure.

2.2.4. Enthalpy and entropy of melting, and densities

To calculate the volumetric and thermodynamic properties of ice and water along the melting lines of ML-BOP and TIP4P/2005, we use previously made single phase ice Ih and water simulation cells with 9216 and 8000 water molecules, respectively. Ice and water boxes are individually equilibrated at the melting temperatures and pressures for 2 ns for the ML-BOP and 0.2 ns for TIP4P/2005. The equilibrated configurations are then used for a production simulation to collect the density and enthalpy data. These production simulations are last for 5 ns for water and 2 ns for ice for the ML-BOP model, and 2 ns for water and 0.2 ns for ice for TIP4P/2005. The enthalpy of melting is the difference between the enthalpy of liquid and ice; $\Delta H_{melt} = H_{liq}(T_m) - H_{ice}(T_m)$. The entropy of melting is $\Delta S_{melt} = \frac{\Delta H_{melt}}{T_m}$, where T_m is the melting temperature of ice Ih.

2.2.5. Homogeneous crystallization temperature.

We estimate the temperatures of maximum crystallization rate as a function of pressure for the ML-BOP model in the -150-300 MPa range. Starting from an equilibrium liquid configuration at 278 K at 0.1MPa, we cool the system at a rate of 10 K/ns, 4 K/ns, 1 K/ns, 0.5 K/ns, 0.2 K/ns, 0.1 K/ns, and 0.05 K/ns. We observe that a rate of 0.2 K/ns or below ML-BOP water spontaneously crystallizes to ice (Supp. Info. Figure S2). Above that specified rate the system vitrifies instead of crystallizing.

We use the CHILL+ algorithm to identify the nucleation and growth of ice in simulations.[74, 75] The temperature at which a stable ice nucleus starts growing is defined to be the homogeneous crystallization temperature, T_h. We then fixed the cooling rate to 0.2 K/ns for the crystallization of ice Ih at all other pressures. Once we get the T_h value from one cooling simulation at a given pressure, we equilibrate the supercooled water 20 K above that T_h and generate 5 restart files. These restart files with different initial configurations and velocities are then used for cooling simulations to find the individual T_h values. The T_h values of all these 5 independent cooling simulations along with the one performed before are then averaged to get the final T_h. Standard error from these 6 independent simulations are presented as error bar in the $T_h(p)$ curve shown in Section 3.3. We follow a similar protocol for all other pressures, except that we perform a total of 11 independent cooling simulations at -100 MPa and -150 MPa. This is because some cooling simulations fail to produce enough amount of ice in the simulation box to distinguish nucleation and growth events. Out of these total 11 cooling simulations, we choose 6 where we see an identifiable nucleation and growth event. This enhances the accuracy of our estimation of T_h at lower pressures.

2.2.6. Cavitation pressure.

We further calculate the cavitation pressures at different temperatures in the ML-BOP model. First, we equilibrate the liquid water at -40 MPa pressures at different temperatures ranging from 178 to 318 K. We then decrease the pressure of the system with a rate of rate 10 bar ns^{-1}. The pressure at which the extended liquid first breaks to form

liquid and vapor phases is recorded as the cavitation pressure, P_{cav} at the corresponding temperature.

3. RESULTS AND DISCUSSION

3.1. ML-BOP captures the change between local orders in water with pressure and temperature.

The first peak in oxygen-oxygen radial distribution function in liquid water corresponds to the hydrogen bonding distance between water molecules. Figure 1a-b show the radial distribution function and corresponding structure factor for ML-BOP, TIP4P/2005 and experiments at 298 K and ambient pressure. Overall, ML-BOP captures the characteristic features of the oxygen-oxygen RDF and structure factors of water, despite the lack of any structural information in the parameterization of the model (Figure 1a). However, there are some differences with the experiment. First, ML-BOP overestimates the height of first peak of the RDF, like TIP4P/2005 and other rigid non-polarizable water models,[2, 3, 27] suggesting a narrower distribution of local orders compared to water. Second, ML-BOP predicts that the first neighbor shell peaks at slightly larger distances than in the experiment (2.84 vs 2.807 Å[76]). Third, the gap between the first and second solvation shells is more pronounced in ML-BOP. Interestingly, this is also the case for TIP4P/Ice,[3] although the gap is more pronounced in the coarse-grained model and originates on the choice of switching (R-D = 3.01 Å) and cutoff (R+D = 3.55 Å) distances in the pair interaction energy of ML-BOP (Eq. 2).[13, 57] These two distances are shown with vertical dashed lines in Figure 1a. The pronounced separation between first and second solvation shell is also visible in the lower height of the pre-peak in the oxygen-oxygen structure factor (Figure 1b). Despite these discrepancies, ML-BOP reproduces well the number of water neighbors in the first solvation shell at ambient conditions.[13]

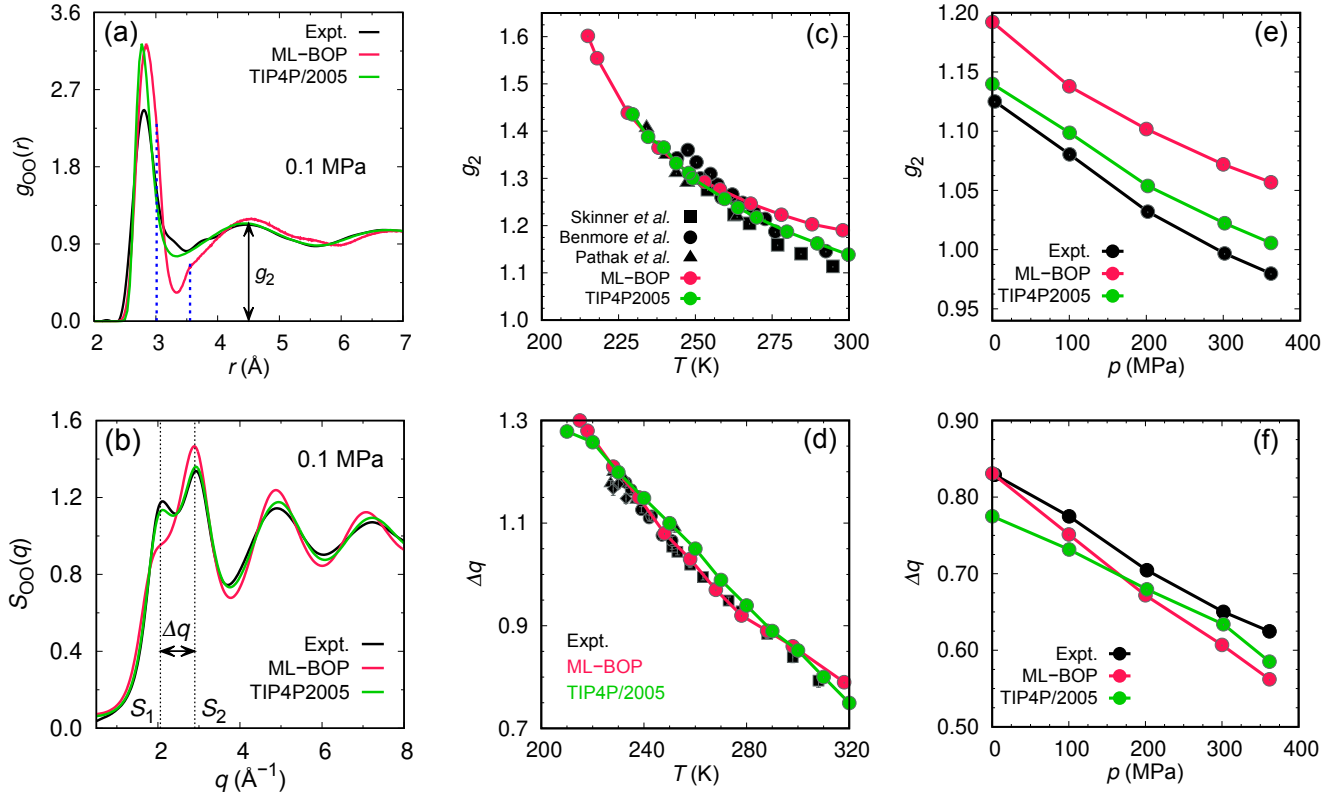

Figure 1. Comparison of the structure of liquid ML-BOP, TIP4P/2005 and water. (a) Radial distribution function, $g_{OO}(r)$, between water oxygens at 0.1 MPa and 298 K in liquid water in experiments[76] (black), ML-BOP (red) and TIP4P/2005 (green). The height of the second peak, g_2 is shown with a two-headed arrow. The vertical blue dashed lines signal the position of the switching (R-D) and cutoff (R+D) distances in the ML-BOP potential. b) Structure factor, $S_{OO}(q)$ at 0.1 MPa and 298 K, (same colors as in a). The principal peak splits into sub-peaks at S_1 and S_2 (dotted black vertical lines) Δq apart. Supp. Info. Figure S3 shows the RDFs and $S(q)$s of ML-BOP at 0.1 MPa for temperatures ranging from 215 K to 318 K. (c) Temperature dependence of g_2 in ML-BOP at 0.1 MPa agrees well with the data from experiments[27, 77-79] and simulations with the TIP4P/2005 model.[27] (d) Temperature dependence of Δq at 0.1 MPa for ML-BOP is in excellent agreement with the experiment.[26] (e) Pressure dependence of g_2 for liquid ML-BOP, TIP4P/2005 and water[76] at 298 K. (f) Splitting Δq of the first peak in the structure factor at 298 K as a function of pressure for ML-BOP, TIP4P/2005 and water.[76]. Supp. Info. Figure S4 shows the RDF and $S(q)$ of ML-BOP and TIP4P/2005 as a function of pressure.

The position of the second peak of the radial distribution function between water oxygens corresponds to the distance between these atoms in a tetrahedron. Its height g_2 (Figure 1a) has been used as a measure of the tetrahedrality of liquid water.[26] The evolution of g_2 with temperature has been used to measure the performance of water models.[27, 28,

[80] g_2 vs temperature at 0.1 MPa has been reported for a wide variety of models, including mW, TIP4P/2005, SPC/E, TIP5P and MB-Pol.[27, 28] It was found that TIP4P/2005 and MB-Pol display very good agreement with the experimental data.[27] Figure 1c shows g_2 vs temperature for ML-BOP, together with the results of TIP4P/2005[27] and water.[27,73-75] ML-BOP overestimates g_2 of water at 298 K by 6%, but it is in quantitative agreement with the experiment below 265 K (Figure 1c). It is noteworthy that ML-BOP reproduces the sharp increase in the tetrahedrality of liquid water in the supercooled region, even at temperatures below the 253 K lower boundary used in the parameterization of the model.

The split $\Delta q = S_2 - S_1$ of the principal peak in the static structure factor of water (Figure 1b) has been related, like g_2, the to an increase in the structural ordering of water.[26] Figure 1d shows that ML-BOP reproduces the temperature dependence of Δq in experiments[26] with even more accuracy than TIP4P/2005.[27] Supp. Info Figure S5 shows that the excellent agreement originates on the ability of ML-BOP to replicate the temperature dependence of S_1 and S_2. We conclude that ML-BOP correctly represents the increase in population of tetrahedral-like order in liquid water upon cooling at room pressure.

Can ML-BOP capture the pressure dependence of the tetrahedral-like populations in water, despite being parameterized with data of the liquid at 0.1 MPa? Figure 1e-f presents g_2 and Δq of liquid water at 298 K from 0.1 to 350 MPa together with the predictions of ML-BOP and TIP4P/2005. To our knowledge, this is the first comparison of g_2 and Δq for any water model as a function of pressure. Both quantities decrease with pressure, consistent with a weakening of the tetrahedral network of water.[26]

ML-BOP and TIP4P/2005 reproduce well the slope of g_2 and Δq of water a function of at 298 K. Nevertheless, $g_2(p)$ of ML-BOP is systematically 6 to 7.5% higher than for water upon compression at room temperature (Figure 1d). We are not aware of experimental g_2 for supercooled water at high pressure. However, the results in Figure 1c show that ML-BOP and TIP4P/2005 produce identical g_2 = 1.31 at 248 K and 0.1 MPa. Hence, we compute this property for these two models at 248 K and a high pressure, 362 MPa, and find them to be both g_2 = 1.083, identical again. We conclude that ML-BOP reproduces well the pressure and temperature dependence of the second peak of the RDF that signals tetrahedral-like order in water.

The results above raise the question of what is the effect of temperature and pressure on the microscopic configurations of ML-BOP. The angular distribution function $P(\theta)$ between triplets of neighboring waters is not directly accessible through experiments but is a good proxy to investigate local order in water across water models. All water models display two distinct populations in the angular distribution $P(\theta)$ between oxygen atoms: one peak centered around θ = 100° that corresponds to a broad distribution of distorted tetrahedral configurations, and another around 60° that corresponds to closed packed configurations. This is also the case for ML-BOP (Figure 2a,c).

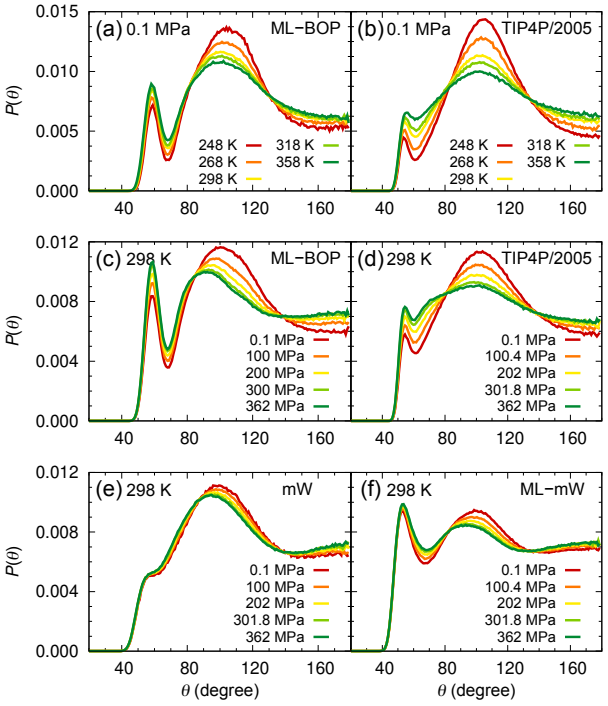

Figure 2. Temperature and pressure dependence of the angular distribution in liquid water. The temperature and pressure dependence of angular distribution function (ADF) of water oxygens in (a) ML-BOP, (b) TIP4P/2005, (c) mW, and (d) ML-mW. Supporting Figure S7 shows that even though the ADFs of ML-BOP and TIP4P/2005 are not same within the first coordination shell, with increase in the size of the first shell cutoff both the models become very close.

The peaks of closed-packed and tetrahedral-like order in ML-BOP and TIP4P/2005 have comparable sensitivity to temperature (Figure 2a-b) and pressure (Figure 2c-d). Interestingly, ML-BOP has a larger fraction of close-packed water triplets compared to TIP4P/2005, despite having an angular form $g(\theta)$ that penalizes more the low angles of closed packed triplets (Supp. Fig. S6). Moreover, the tetrahedral-like peak of ML-BOP responds to increase in either pressure or temperature by shifting to lower angles, while the tetrahedral-like peak of TIP4P/2005 not only shifts but also broadens upon heating and compression. Even at conditions for which ML-BOP and TIP4P/2005 have identical g_2 (Figure 1c), the CG and AA models sample different angular distributions in the supercooled liquid (Figure 2a-b and Supp Figure S8). The difference in microscopic configurations between ML-BOP and water become more pronounced on compression. Inspection of the RDF at 248 K (Supp Figures S8c-d) suggests that ML-BOP can capture the structure of low-density amorphous ice upon cooling at low pressure, but fails at reproducing the collapse of the second shell into the

first one that is typical of high-density amorphous ice in experiments and all-atom models at high pressures.[81-84]

We find that the microscopic configurations of Stillinger-Weber (SW) models of water have lower sensitivity to pressure than ML-BOP. Figure 2e-f presents $P(\theta)$ as a function of pressure for mW and ML-mW at 298 K. The latter was parameterized with the same machine learning method and training set as the ML-BOP model.[13] While mW and ML-mW have quite different proportions of closed-packed and tetrahedral configurations, both SW models underestimate the change in $P(\theta)$ with pressure. The low impact of pressure on the populations of the SW water models correlates with their lower slope of g_2 with temperature[28] and pressure (Sup. Fig. S9). We conclude that it is the functional flexibility of the Tersoff potential, and not only its exhaustive parameterization procedure and training set, that endows ML-BOP with the structural sensitivity to pressure and temperature comparable to that of TI4P/2005 and water.

3.2. ML-BOP reproduces the pressure dependence of the melting line and EOS of water and ice.

The melting temperature of the newly developed machine-learned coarse-grained model ML-BOP at 0.1 MPa was found to be 273 ± 1 K in two-phase simulations with a time step of 10 fs and a cell with 720 molecules.[13] It has been shown before that the estimation of T_m using the coexistence method is sensitive to the size of the simulation cell and the time step of the simulation.[55, 56] Using a simulation box with 9216 water molecules and a time step of 5 fs, we find T_m = 279.5 ± 1 K, within 2.3% of the experimental value 0.1 MPa.

A recent comparative study of water models[85] reported that the only ones that reproduce T_m within 3 K of the experimental value at 0.1 MPa are the monatomic model mW (T_m = 273.0 ± 0.5 K[55]) the four-site model TIP4P/Ice (T_m = 270 ± 3 K[3]), the five site models TIP5P (T_m = 274 ± 1 K[85]) and TIP45P/Ew (T_m = 271 ± 3 K[86]), and the six-site model TIP6P-Ew (T_m = 274.5 ± 1.5 K[87]). However, each model in that set have temperature of maximum density (TMD) at least 20 K apart from their T_m,[85] while in experiment TMD = 277 K is just 4 K above T_m = 273.15 K at 0.1 MPa bar. The polarizable models MB-Pol (T_m = 263.5 ± 1.5 K[8], TMD = 263 K[8]) and the coarse-grained model ML-BOP are the only water models that predict TMD within 5 K of T_m.

We note that for ML-BOP the TMD is below the melting line, same as also for the monatomic mW[11] and ML-mW,[13] as well as the all-atom flexible TIP4P/FQ[85] and – marginally- MB-POL[8] models. That ordering is opposite to what is found in water and the majority of all-atom water models.[85] Even with the upwards-updated value of T_m for ML-BOP presented here, this monatomic model displays better overall agreement with experiments in T_m (279.5 ± 1 *vs* 273.15 K) and TMD (276 ± 1[13] *vs* 277 K) than any other atomistic or coarse-grained water model developed to date.

Figure 3a reveals that ML-BOP reproduces the experimental pressure-dependent melting line of ice I with accuracy 0.5 to 2.3% across the whole experimental range, from 0.1 to 200 MPa, and its extrapolation with an accurate equation of state (EOS) to 400 MPa.[50, 88, 89] $T_m(p)$ of the coarse-grained ML-BOP model is significantly more accurate than for TIP4P/2005[2], and comparable to that of the TIP4P/Ice, which was parameterized to reproduce the ice-liquid-equilibrium.[3]

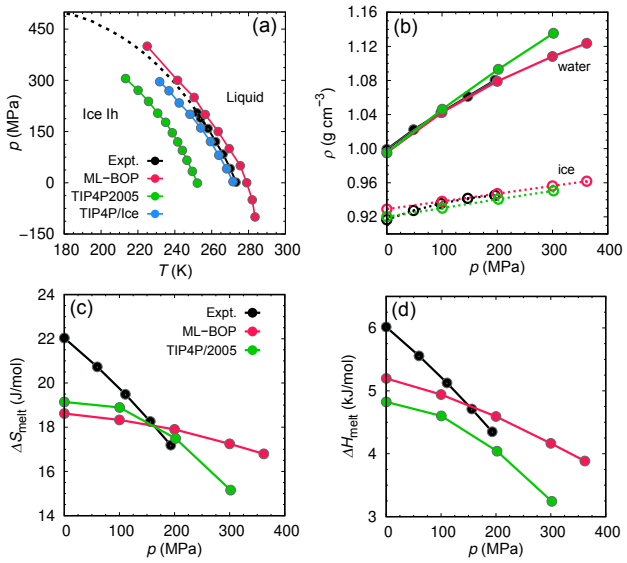

Figure 3. ML-BOP reproduces the ice Ih-liquid equilibrium properties of water. (a) The melting line of ice Ih calculated from ML-BOP (red) model is within 2.3% of the experimental and equation of state values[2, 50] (black) at pressures up to 400 MPa pressure. Solid black line-points represent the coexistence line where ice Ih is the stable phase below T_m. The dashed black line in (a) is the metastable extension of the experimental melting line of ice Ih calculated with the equation of state (EOS) of ice and supercooled water,[50] which reproduces accurately the high-pressure T_m data. TIP4P/2005 (green) underestimates T_m but reproduces the slope with pressure. TIP4P/Ice (blue) maintains the slope of $T_m(p)$ and matches with the experiment with the same accuracy as ML-BOP. The data of the TIP4P/2005 and TIP4P/Ice models are taken from Ref.[2] and Ref.[3] respectively. (b) Density of liquid water (solid line-points) and ice Ih (open line-points) for the ML-BOP (red) and TIP4P/2005 (green) models along the corresponding melting curves. The experimental data are taken from Ref.[90] Pressure dependence of (c) the entropy of melting and (d) the enthalpy of melting of ML-BOP, TIP4P/2005 and water. The experimental ΔH_{melt} data are taken from Ref.[91] ΔS_{melt} is computed as $\Delta H_{melt}/T_m$.

To understand why ML-BOP is so accurate at reproducing $T_m(p)$, we express its slope with the Clausius-Clapeyron equation,

$$\left(\frac{dT}{dp}\right)_{melt} = \frac{\Delta V_{melt}}{\Delta S_{melt}}, \qquad (9)$$

where ΔV_{melt} and ΔS_{melt} are the volume and entropy changes upon melting. ML-BOP predicts a slope of the melting line at 0.1 MPa[13] within 3% of the experimental value. Here we focus on the evolution of ΔV_{melt} and ΔS_{melt} along the melting line. The equation of state $\rho(T,p)$ of liquid

and ice ML-BOP at 0.1 MPa faithfully represents the one of water. This accuracy is preserved at high pressures. Figure 3b shows that ML-BOP reproduces the experimental density[90] of liquid water and ice along the melting line from 0.1 to 200 MPa within 0.3% and 1.3% of the experimental values.[90] This accuracy is unprecedented among coarse-grained models (Supp. Info. Figure S10). TIP4P/2005 predicts densities for ice and liquid at its own depressed $T_m(p)$ in close agreement with the ones of water at its $T_m(p)$ (Figure 3b). The density of liquid TIP4P/2005 evaluated at the experimental $T_m(p)$ is 0.15% higher than experiment at 0.1 MPa and 0.6% at 200 MPa. We note that ML-BOP and TIP4P/2005 are both extremely accurate in the prediction of $\rho(T)$ of water at 0.1 MPa.[13] This is a non-trivial achievement, as ML-mW –which was parameterized with the same training set and procedure as ML-BOP but is based on the Stillinger-Weber functional form- does not quantitatively reproduce $\rho(T)$ of water at 0.1 MPa.[13] We conclude that ML-BOP reproduces the EOS of water across the supercooled and compressed region with high accuracy, comparable to that of TIP4P/2005.

The entropy of melting ΔS_{melt} for ice Ih does not differ significantly among water models, irrespective of whether they are all-atom or coarse-grained.[13, 33] It has been argued that the insensitivity stems from a small rotational contribution to the entropy of melting of ice, absent in monatomic models.[45] At ambient pressure, ΔS_{melt} of ML-BOP lies within 2.7% of that for TIP4P/2005 and 14.2% below the experiments. Same as for the volumes, the agreement improves with pressure and is near quantitative at 200 MPa (Figure 3c). We note that an accurate representation of the change in entropy on compression hinges on a good description of the equation of state, as these are related by $(dV/dT)_p = -(dS/dp)_T$. Likewise, accuracy in the EOS of liquid and ice is probably at the heart of the good account of the change in the enthalpy of melting with pressure, $\Delta H_{melt}(p) = T_m(p)\,\Delta S_{melt}(p)$ by ML-BOP (Figure 2d). We conclude that the coarse-grained model ML-BOP replicates the thermodynamics of ice-liquid equilibrium as a function of pressure with an accuracy that rivals that of the best water models.

It is interesting to note that liquid ML-BOP and TIP4P/2005 do not sample exactly the same configurations (Figure 2a-d), but they nevertheless have almost identical equations of state (EOS). This can be understood in terms of the two-state thermodynamics of water, which posits that the liquid is composed of populations of two structural "components" that interconvert as a function of pressure and temperature according to non-ideal mixing thermodynamics.[92, 93] The identity of these structural motifs is irrelevant to the thermodynamic behavior. Only the thermodynamic properties of these motifs and their interconversion with p and T driven by their energies, volumes and non-ideality of their interaction matters to produce the EOS. We interpret that the success of ML-BOP in representing the EOS of water mostly stems from an accurate dependence with temperature and pressure of the interconversion of the populations that represent the high-temperature denser and low-temperature lighter orders in the liquid.

3.3.Region of metastability of liquid water in the ML-BOP model

The accurate prediction of the pressure dependence of the thermodynamic of ice-liquid equilibrium by the ML-BOP model implies that a monatomic representation of water based on very short-range interactions can accurately capture its phase behavior throughout all the range of pressures of ice I. We now focus on establishing the kinetic limits of metastability of supercooled liquid ML-BOP with respect to crystallization and cavitation.

Figure 4 shows the extended phase diagram of water and ML-BOP, including the equilibrium melting lines, together with the non-equilibrium homogeneous ice nucleation and cavitation lines. The temperature of homogeneous nucleation of ice T_h is a kinetic property that depends on the rate at which water is cooled and the volume of the sample. The blue filled triangles in Figure 4 show the $T_h(p)$ line computed in isobaric simulations with a cooling rate of 0.2 K ns^{-1}, which is about the fastest rate that results in spontaneous ice formation with a ~250 nm^3 simulation cell in this model. The higher diffusivity and lower fragility of ML-BOP compared to water,[13] allows for the equilibration of the liquid in these cooling simulations down to the crystallization temperature. The ice nucleation temperature in our simulations is -as expected- lower than in the experiments of Kanno and Angell[94] with 22 orders of magnitude larger droplets at a cooling rate of 3 K min^{-1} (open blue triangles in Figure 4). The widening gap between $T_h(p)$ and $T_m(p)$ with increasing pressure in ML-BOP is similar to that of the coarse-grained mW water model[56] and qualitatively consistent with the behavior of water in experiments.[50, 94] However, the gap between $T_h(p)$ and $T_m(p)$ is less sensitive to pressure in ML-BOP compared to water, and widens significantly only upon approaching ~300 MPa.

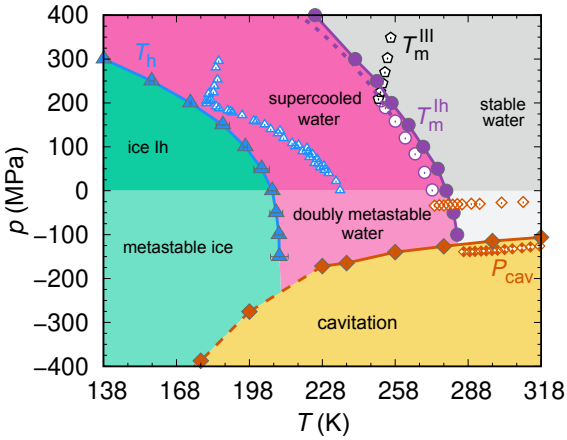

Figure 4. Temperature-pressure ranges of stability and metastability of liquid water in the ML-BOP model and experiments. Filled symbols

correspond to ML-BOP and open symbols to water. The melting line $T_m(p)$ of ice Ih is shown in violet, the homogeneous crystallization line $T_h(p)$ in blue, and the cavitation line $P_{cav}(T)$ in orange. The experimental melting, crystallization and cavitation lines are taken from Ref.[64], Ref.[94] and Ref.[64, 95, 96] respectively. The experimental cavitation line obtained by acoustical measurements[63, 94] is shown with empty orange diamonds and the one obtained from microscopic inclusions[96] with half-empty orange diamonds. The dashed violet line is the metastable extension of the experimental melting line of ice Ih calculated with the equation of state (EOS) of ice and supercooled water,[50] which reproduces accurately the high-pressure T_m data. The experimental water-ice III equilibrium line is shown with open black pentagons.[2] Note that P_{cav} at 178 K and 198 K for ML-BOP correspond to cavitation of non-equilibrated amorphous viscous water, whereas for other temperatures cavitation occurs from the stable or metastable equilibrated liquid.

Supercooled liquid ML-BOP spontaneously nucleates and grows ice I at pressures up to 300 MPa (Figure 2). The liquid does not crystallize when cooled at pressures between 300 to 600 MPa, even at rates as low as 0.05 K ns^{-1}. However, when cooled at that rate at 800 MPa it crystallizes at 98 K to 6-coordinated β-tin at 98 K, which is not a high-pressure phase of ice. That representability issue is shared with other monatomic models of water: the SW coarse-grained water models mW and mTIP4P/2005^{REM} [33] crystallize to ice I at moderate pressures, but produce the four-coordinated non-tetrahedral sc16 structure at higher pressures.[56, 97] It is an open question whether other monatomic water models with different interaction form would be able to reproduce the high pressure phases of ice or the limitation is intrinsic to the symmetry that results from the lack of explicit hydrogen atoms.

The Clausius-Clapeyron relation (Eq 9) together with the pressure dependence of ΔH_{melt} and ΔV_{melt} (Figure 2), predict that the $T_m(p)$ line would become reentrant beyond when the density of the liquid becomes lower than that of ice I. This condition is anticipated to occur at negative pressures but is never met in the experiments nor in simulations with the ML-BOP model, because the liquid cavitates as ΔV_{melt} approaches zero. The fast expansion rates and smaller volumes of the simulation cells allow for extension along the melting line to $p \approx$ -120 MPa, about thrice the $p \approx$ -35 MPa[64, 95] (Figure 4) that can be attained before cavitation at the melting temperature in experiments with several orders of magnitude larger samples and slower expansion rates.

We note that ML-BOP reproduces well the experimental slope of $P_{cav}(T)$ (compare the orange filled with the empty or half-empty orange symbols in Figure 4). The cavitation line of the model occurs at more negative pressures that the one measured by acoustic measurements,[63, 94] and close to the cavitation line obtained by isochoric cooling of water in microscopic inclusions.[65, 96, 98, 99] The smaller volumes and faster expansion used in the simulations allow for the sampling of $P_{cav}(T)$ down to temperatures well below the crystallization line $T_h(p)$, where the slow relaxation of the supercooled liquid slows down the coarsening of ice in the simulation. The region where $T_h(p)$ and $P_{cav}(T)$ cross is the most challenging to characterize because of the competition between fast cavitation and fast ice crystallization of the doubly metastable liquid.

It has been previously shown that the sign of the slope of the crystallization line $T_h(p)$ follows that of the melting line $T_m(p)$ for the mW and mTIP4P/2005^{REM} monatomic SW water models,[56] as well as the all-atom TIP4P/2005[100], TIP4P,[51] and TIP4P/Ice,[101] and other liquids with water-like anomalies.[102] The same is observed for ML-BOP, for which $dT_h/dp = 0$ at $p \approx$ -150 MPa (Figure 4). The closeness in reentrant pressures for $T_h(p)$ and $T_m(p)$ seems to be a common characteristic of all water-like liquids.

4. CONCLUSIONS AND OUTLOOK

The monatomic machine learned ML-BOP model is a parameterization of the Tersoff potential optimized using a multilevel evolutionary strategy.[13] The lack of hydrogen atoms and extremely short-range nature of the interatomic potential, just 3.55 Å, makes ML-BOP 100 times computationally more efficient than rigid non-polarizable all-atom models, such as TIP4P/2005 and TIP4P/Ice.[13] In this study, we characterize the structure of stable and supercooled ML-BOP liquid, and its thermodynamics at the water-ice equilibrium line across all the range of pressures of ice I.

We find that ML-BOP accurately reproduces the equilibrium melting line of ice Ih at pressures up to 400 MPa with accuracy higher than TIP4P/2005 and equal to TIP4P/Ice. We note that these two AA models were parameterized to reproduce experimental properties of water and ice in a wide range of temperatures and pressures,[2, 3] and the parameters of TIP4P/Ice were specifically selected to reproduce the ice-liquid equilibrium properties.[3] ML-BOP, on the other hand, was parameterized with experimental densities of ice and water at 0.1 MPa over a wide range of temperatures together with the stress-strain response of TIP4P/2005 ice at 0 K.[13] The accuracy of $T_m(p)$ in ML-BOP hinges on its ability to closely track the experimental volume and entropy of melting along all the region of stability of ice I.

The parameterization of ML-BOP did not involve structural information such as radial or angular distributions in the training data.[13] We find that while ML-BOP reproduces well the thermodynamics of water, the microscopic states sampled by the coarse-grained model in the liquid are not identical to those of water or TIP4P/2005. While the radial distribution function of ML-BOP is quite similar to water, further inspection of the three-body angular distribution functions reveal that ML-BOP has a higher fraction of closed packed configurations than TIP4P/2005, and its tetrahedral-like peak shifts to lower angles under pressure instead of broadening as in the all-atom model. Nevertheless, the rate of change in populations in ML-BOP and TIP4P/2005 with pressure and temperature seem to be comparable, suggesting that these models have similar two-state thermodynamics,

despite the different identity of the two interconverting structures that can be used to represent the liquid as a non-ideal mixture model. [20-22, 50]

We demonstrate that ML-BOP reproduces the sharp increase in the tetrahedral peak g_2 of the RDF water upon cooling at 0.1 MPa, as well as its pressure dependence. No monatomic water model characterized to date combines accuracy in the prediction of water thermodynamics and the existence of a liquid-liquid critical point. We note that –same as in water- the simulations of ML-BOP at high pressure result in the crystallization, rather than a liquid-liquid transformation of the supercooled liquid. However, the steepness in the structural changes in ML-BOP with temperature and pressure suggest that the model is a good candidate to have a liquid-liquid transition in the metastable region, hidden behind the crystallization line.

It is remarkable that the coarse-grained model ML-BOP predicts the equation of state of liquid and ice and the thermodynamics of their two-phase equilibrium in par with the most accurate all-atom models. What is the origin of this success? We interpret that the functional form and flexibility of the Tersoff potential, together with the HOGA optimization, allowed not only for unprecedented accuracy in capturing $\rho(T)$ of water and ice at ambient pressure, but also translated these volumetric changes into an accurate sensitivity to temperature of the ratio of closed-packed and open tetrahedral-like configurations in the liquid. Low density local order in water is favored at low temperature, and high density one at high temperature. Hence, the training of the model that captured the dependence of these populations with temperature, imparted a proper response to pressure. The addition of the pressure-volume data of minimized TIP4P/2005 ice I further taught the potential to mimic the compressibility of the perfectly tetrahedral configuration, decoupled from changes in the populations of local orders. To set all the properties of the model, a temperature scale must be added to the EOS properties. ML-BOP achieved that by striving to reproduce the temperature and enthalpy of melting, which provide the cost of transforming the perfectly tetrahedral structure of ice I into the "mixture" of distorted motifs of the liquid. The result is a coarse-grained model with an unprecedented accuracy in reproducing the equation of state of water and ice along a wide range of temperatures and pressures.

The mW and ML-mW water models based on the Stillinger-Weber potential are less accurate than ML-BOP in representing the properties of water.[13, 56] We find that mW and ML-mW models have different proportions of closed packed configurations in the liquid, but both have similar insensitivity of these populations to pressure. As ML-mW was parameterized with the same method as training set as ML-BOP, we conclude that the Stillinger-Weber functional form is too rigid to accommodate the relative changes in populations of open tetrahedral and closed-packed fractions with temperature and pressure required to reproduce the EOS of water. The lack of flexibility of the angular form of SW to represent the structure of water has been previously discussed in the literature.[33] It is an open question what feature of the Tersoff potential –the large number of parameters, the more flexible angular dependence, the embedding of the three-body angular dependence into a bond-order scalong term of the two-body attraction- is responsible for its success at capturing the EOS of water, and whether the functional form of this monatomic model could be modified to also reproduce the experimental structure of liquid water across thermodynamic states.

Understanding the behavior of liquid water in the supercooled and stretched regions is important for establishing the connection between anomalies in water and polyamorphic transformations in the supercooled liquid state. We demarcate the limits of metastability of ML-BOP liquid with respect to crystallization as a function of pressure and temperature. We show that supercooled ML-BOP spontaneously nucleates ice within accessible simulation times along the whole range of pressures of ice I. The crystallization times are accessible because the computational efficiency of the model allows for large scale simulations over hundreds of nanoseconds, the mobility of ML-BOP liquid decreases more slowly than that of water on cooling,[13] increasing the rates of nucleation and growth of ice. The accessibility of ice crystallization to simulations of ML-BOP, together with its accurate representation of the thermodynamics of water, makes it promising for investigating the interplay between anomalies, glass transition, and crystallization of water in simulations where an adequate balance of computational efficiency and accuracy is important.

ACKNOWLEDGMENTS

We are indebted to Henry Chan for insightful discussions on the ML-BOP model and for providing the input file for its implementation in LAMMPS, and grateful to Suvo Banik, Jaehyeok Jin and Frédéric Caupin for discussions and comments. This work was supported by U.S. Air Force Office of Scientific Research through MURI Award FA9550-20-1-0351. We thank the Center of High-Performance Computing at The University of Utah through technical support and an award of computing time.

ASSOCIATED CONTENT

Supporting Information

The Supporting Information is available free of charge at.

Simulation setup for the calculation of melting temperature of ice Ih; identification of maximum crystallization rate using CHILL+; Supplementary plots for the temperature and pressure dependence of $g_{OO}(r)$ and $S_{OO}(q)$; temperature dependence of S_1 and S_2; cutoff-distance dependence in the calculation of ADFs; interatomic angular potential $g(\theta)$ for the three monatomic models considered here; pressure dependence of angular distribution function at 248 K; change in tetrahedrality of monatomic and all-atom water models

with the change in pressure; density of water and Ice Ih along the melting line of mW model.

AUTHOR INFORMATION

Corresponding Author

Valeria Molinero – Department of Chemistry, The University of Utah, Salt Lake City, Utah 84112-0850, United States.

orcid.org/0000-0002-8577-4675;

Email: valeria.molinero@utah.edu

Authors

Debdas Dhabal – Department of Chemistry, The University of Utah, Salt Lake City, Utah 84112-0850, United States.

orcid.org/0000-0003-1534-1599;

Subramanian K.R.S. Shankaranarayanan – Department of Mechanical and Industrial Engineering, University of Illinois, Chicago, Illinois 60607, United States.

Center for Nanoscale Materials, Argonne National Laboratory, Lemont, Illinois 60439, United States.

orcid.org/0000-0002-9708-396X.

ABBREVIATIONS

ML-BOP: Machine-learned bond-order potential; ML-mW: Machine-learned monatomic water; RDFs: Radial distribution function; ADF: Angular distribution function; LLCP: liquid-liquid critical point.

REFERENCES

1. Bernal, J. D.; Fowler, R. H., A Theory of Water and Ionic Solution, with Particular Reference to Hydrogen and Hydroxyl Ions. *The Journal of Chemical Physics* **1933,** *1* (8), 515-548.
2. Abascal, J. L. F.; Vega, C., A general purpose model for the condensed phases of water: TIP4P/2005. *The Journal of Chemical Physics* **2005,** *123* (23), 234505.
3. Abascal, J. L. F.; Sanz, E.; García Fernández, R.; Vega, C., A potential model for the study of ices and amorphous water: TIP4P/Ice. *The Journal of Chemical Physics* **2005,** *122* (23), 234511.
4. Berendsen, H. J. C.; Grigera, J. R.; Straatsma, T. P., The missing term in effective pair potentials. *The Journal of Physical Chemistry* **1987,** *91* (24), 6269-6271.
5. Jorgensen, W. L.; Chandrasekhar, J.; Madura, J. D.; Impey, R. W.; Klein, M. L., Comparison of simple potential functions for simulating liquid water. *The Journal of Chemical Physics* **1983,** *79* (2), 926-935.
6. Cornell, W. D.; Cieplak, P.; Bayly, C. I.; Gould, I. R.; Merz, K. M.; Ferguson, D. M.; Spellmeyer, D. C.; Fox, T.; Caldwell, J. W.; Kollman, P. A., A Second Generation Force Field for the Simulation of Proteins, Nucleic Acids, and Organic Molecules. *Journal of the American Chemical Society* **1995,** *117* (19), 5179-5197.
7. Mahoney, M. W.; Jorgensen, W. L., A five-site model for liquid water and the reproduction of the density anomaly by rigid, nonpolarizable potential functions. *The Journal of Chemical Physics* **2000,** *112* (20), 8910-8922.
8. Reddy, S. K.; Straight, S. C.; Bajaj, P.; Huy Pham, C.; Riera, M.; Moberg, D. R.; Morales, M. A.; Knight, C.; Götz, A. W.; Paesani, F., On the accuracy of the MB-pol many-body potential for water: Interaction energies, vibrational frequencies, and classical thermodynamic and dynamical properties from clusters to liquid water and ice. *The Journal of Chemical Physics* **2016,** *145* (19), 194504.
9. Wang, L.-P.; Head-Gordon, T.; Ponder, J. W.; Ren, P.; Chodera, J. D.; Eastman, P. K.; Martinez, T. J.; Pande, V. S., Systematic Improvement of a Classical Molecular Model of Water. *The Journal of Physical Chemistry B* **2013,** *117* (34), 9956-9972.
10. Lamoureux, G.; Harder, E.; Vorobyov, I. V.; Roux, B.; MacKerell, A. D., A polarizable model of water for molecular dynamics simulations of biomolecules. *Chemical Physics Letters* **2006,** *418* (1), 245-249.
11. Molinero, V.; Moore, E. B., Water Modeled As an Intermediate Element between Carbon and Silicon. *The Journal of Physical Chemistry B* **2009,** *113* (13), 4008-4016.
12. Izadi, S.; Anandakrishnan, R.; Onufriev, A. V., Building Water Models: A Different Approach. *The Journal of Physical Chemistry Letters* **2014,** *5* (21), 3863-3871.
13. Chan, H.; Cherukara, M. J.; Narayanan, B.; Loeffler, T. D.; Benmore, C.; Gray, S. K.; Sankaranarayanan, S. K. R. S., Machine learning coarse grained models for water. *Nature Communications* **2019,** *10* (1), 379.
14. Fuentes-Azcatl, R.; Barbosa, M. C., Flexible bond and angle, FBA/ϵ model of water. *Journal of Molecular Liquids* **2020,** *303*, 112598.
15. Hadley, K. R.; McCabe, C., Coarse-grained molecular models of water: a review. *Molecular Simulation* **2012,** *38* (8-9), 671-681.
16. Kadaoluwa Pathirannahalage, S. P.; Meftahi, N.; Elbourne, A.; Weiss, A. C. G.; McConville, C. F.; Padua, A.; Winkler, D. A.; Costa Gomes, M.; Greaves, T. L.; Le, T. C.; Besford, Q. A.; Christofferson, A. J., Systematic Comparison of the Structural and Dynamic Properties of Commonly Used Water Models for Molecular Dynamics Simulations. *Journal of Chemical Information and Modeling* **2021,** *61* (9), 4521-4536.
17. Cisneros, G. A.; Wikfeldt, K. T.; Ojamäe, L.; Lu, J.; Xu, Y.; Torabifard, H.; Bartók, A. P.; Csányi, G.; Molinero, V.; Paesani, F., Modeling Molecular Interactions in Water: From Pairwise to Many-Body Potential Energy Functions. *Chemical Reviews* **2016,** *116* (13), 7501-7528.
18. Gallo, P.; Amann-Winkel, K.; Angell, C. A.; Anisimov, M. A.; Caupin, F.; Chakravarty, C.; Lascaris, E.; Loerting, T.; Panagiotopoulos, A. Z.; Russo, J.; Sellberg, J. A.; Stanley, H. E.; Tanaka, H.; Vega, C.; Xu, L.; Pettersson, L. G. M., Water: A Tale of Two Liquids. *Chemical Reviews* **2016,** *116* (13), 7463-7500.
19. Leven, I.; Hao, H.; Das, A. K.; Head-Gordon, T., A Reactive Force Field with Coarse-Grained Electrons for Liquid Water. *The Journal of Physical Chemistry Letters* **2020,** *11* (21), 9240-9247.
20. Holten, V.; Limmer, D. T.; Molinero, V.; Anisimov, M. A., Nature of the anomalies in the supercooled liquid state of the mW model of water. *The Journal of Chemical Physics* **2013,** *138* (17), 174501.
21. Holten, V.; Palmer, J. C.; Poole, P. H.; Debenedetti, P. G.; Anisimov, M. A., Two-state thermodynamics of the ST2 model for supercooled water. *The Journal of Chemical Physics* **2014,** *140* (10), 104502.
22. Biddle, J. W.; Singh, R. S.; Sparano, E. M.; Ricci, F.; González, M. A.; Valeriani, C.; Abascal, J. L. F.; Debenedetti, P. G.; Anisimov, M. A.; Caupin, F., Two-structure thermodynamics for the TIP4P/2005 model of water covering supercooled and deeply stretched regions. *The Journal of Chemical Physics* **2017,** *146* (3), 034502.
23. Moore, E. B.; Molinero, V., Growing correlation length in supercooled water. *The Journal of Chemical Physics* **2009,** *130* (24), 244505.
24. Dhabal, D.; Wikfeldt, K. T.; Skinner, L. B.; Chakravarty, C.; Kashyap, H. K., Probing the triplet correlation function in liquid water by experiments and molecular simulations. *Physical Chemistry Chemical Physics* **2017,** *19* (4), 3265-3278.

25. Prasad, S.; Chakravarty, C., Tuning the tetrahedrality of the hydrogen-bonded network of water: Comparison of the effects of pressure and added salts. *The Journal of Chemical Physics* **2016,** *144* (23), 234509.
26. Sellberg, J. A.; Huang, C.; McQueen, T. A.; Loh, N. D.; Laksmono, H.; Schlesinger, D.; Sierra, R. G.; Nordlund, D.; Hampton, C. Y.; Starodub, D.; et al, Ultrafast X-ray probing of water structure below the homogeneous ice nucleation temperature. *Nature* **2014,** *510* (7505), 381-384.
27. Camisasca, G.; Pathak, H.; Wikfeldt, K. T.; Pettersson, L. G. M., Radial distribution functions of water: Models vs experiments. *The Journal of Chemical Physics* **2019,** *151* (4), 044502.
28. Pathak, H.; Palmer, J. C.; Schlesinger, D.; Wikfeldt, K. T.; Sellberg, J. A.; Pettersson, L. G. M.; Nilsson, A., The structural validity of various thermodynamical models of supercooled water. *The Journal of Chemical Physics* **2016,** *145* (13), 134507.
29. Marrink, S. J.; Risselada, H. J.; Yefimov, S.; Tieleman, D. P.; de Vries, A. H., The MARTINI Force Field: Coarse Grained Model for Biomolecular Simulations. *The Journal of Physical Chemistry B* **2007,** *111* (27), 7812-7824.
30. Johnson, M. E.; Head-Gordon, T.; Louis, A. A., Representability problems for coarse-grained water potentials. *The Journal of Chemical Physics* **2007,** *126* (14), 144509.
31. Wang, H.; Junghans, C.; Kremer, K., Comparative atomistic and coarse-grained study of water: What do we lose by coarse-graining? *The European Physical Journal E* **2009,** *28* (2), 221-229.
32. Jacobson, L. C.; Kirby, R. M.; Molinero, V., How Short Is Too Short for the Interactions of a Water Potential? Exploring the Parameter Space of a Coarse-Grained Water Model Using Uncertainty Quantification. *The Journal of Physical Chemistry B* **2014,** *118* (28), 8190-8202.
33. Lu, J.; Qiu, Y.; Baron, R.; Molinero, V., Coarse-Graining of TIP4P/2005, TIP4P-Ew, SPC/E, and TIP3P to Monatomic Anisotropic Water Models Using Relative Entropy Minimization. *Journal of Chemical Theory and Computation* **2014,** *10* (9), 4104-4120.
34. Chaimovich, A.; Shell, M. S., Anomalous waterlike behavior in spherically-symmetric water models optimized with the relative entropy. *Physical Chemistry Chemical Physics* **2009,** *11* (12), 1901-1915.
35. Hadley, K. R.; McCabe, C., On the Investigation of Coarse-Grained Models for Water: Balancing Computational Efficiency and the Retention of Structural Properties. *The Journal of Physical Chemistry B* **2010,** *114* (13), 4590-4599.
36. Wu, Z.; Cui, Q.; Yethiraj, A., A New Coarse-Grained Model for Water: The Importance of Electrostatic Interactions. *The Journal of Physical Chemistry B* **2010,** *114* (32), 10524-10529.
37. Riniker, S.; van Gunsteren, W. F., A simple, efficient polarizable coarse-grained water model for molecular dynamics simulations. *The Journal of Chemical Physics* **2011,** *134* (8), 084110.
38. Darré, L.; Machado, M. R.; Pantano, S., Coarse-grained models of water. *Wiley Interdisciplinary Reviews: Computational Molecular Science* **2012,** *2* (6), 921-930.
39. Jin, J.; Pak, A. J.; Han, Y.; Voth, G. A., A new one-site coarse-grained model for water: Bottom-up many-body projected water (BUMPer). II. Temperature transferability and structural properties at low temperature. *The Journal of Chemical Physics* **2021,** *154* (4), 044105.
40. Stillinger, F. H.; Weber, T. A., Computer simulation of local order in condensed phases of silicon. *Physical Review B* **1985,** *31* (8), 5262-5271.
41. Dhabal, D.; Chakravarty, C.; Molinero, V.; Kashyap, H. K., Comparison of liquid-state anomalies in Stillinger-Weber models of water, silicon, and germanium. *The Journal of Chemical Physics* **2016,** *145* (21), 214502.
42. Dhabal, D.; Nguyen, A. H.; Singh, M.; Khatua, P.; Molinero, V.; Bandyopadhyay, S.; Chakravarty, C., Excess entropy and crystallization in Stillinger-Weber and Lennard-Jones fluids. *The Journal of Chemical Physics* **2015,** *143* (16), 164512.
43. Shadrack Jabes, B.; Nayar, D.; Dhabal, D.; Molinero, V.; Chakravarty, C., Water and other tetrahedral liquids: order, anomalies and solvation. *Journal of Physics: Condensed Matter* **2012,** *24* (28), 284116.
44. Limmer David, T.; Chandler, D., Theory of amorphous ices. *Proceedings of the National Academy of Sciences* **2014,** *111* (26), 9413-9418.
45. Moore, E. B.; Molinero, V., Structural transformation in supercooled water controls the crystallization rate of ice. *Nature* **2011,** *479* (7374), 506-508.
46. Moore, E. B.; Molinero, V., Ice crystallization in water's "no-man's land". *The Journal of chemical physics* **2010,** *132* (24), 244504.
47. Lupi, L.; Hudait, A.; Peters, B.; Grünwald, M.; Gotchy Mullen, R.; Nguyen, A. H.; Molinero, V., Role of stacking disorder in ice nucleation. *Nature* **2017,** *551* (7679), 218-222.
48. Moore, E. B.; Molinero, V., Is it cubic? Ice crystallization from deeply supercooled water. *Physical Chemistry Chemical Physics* **2011,** *13* (44), 20008-20016.
49. Matsumoto, M.; Saito, S.; Ohmine, I., Molecular dynamics simulation of the ice nucleation and growth process leading to water freezing. *Nature* **2002,** *416* (6879), 409-413.
50. Holten, V.; Sengers, J. V.; Anisimov, M. A., Equation of State for Supercooled Water at Pressures up to 400 MPa. *Journal of Physical and Chemical Reference Data* **2014,** *43* (4), 043101.
51. Sanz, E.; Vega, C.; Abascal, J. L. F.; MacDowell, L. G., Phase Diagram of Water from Computer Simulation. *Physical Review Letters* **2004,** *92* (25), 255701.
52. Babin, V.; Leforestier, C.; Paesani, F., Development of a "first principles" water potential with flexible monomers: Dimer potential energy surface, VRT spectrum, and second virial coefficient. *Journal of chemical theory and computation* **2013,** *9* (12), 5395-5403.
53. Pham, C. H.; Reddy, S. K.; Chen, K.; Knight, C.; Paesani, F., Many-Body Interactions in Ice. *Journal of Chemical Theory and Computation* **2017,** *13* (4), 1778-1784.
54. Abascal, J. L. F.; Vega, C., Widom line and the liquid–liquid critical point for the TIP4P/2005 water model. *The Journal of Chemical Physics* **2010,** *133* (23), 234502.
55. Hudait, A.; Qiu, S.; Lupi, L.; Molinero, V., Free energy contributions and structural characterization of stacking disordered ices. *Physical Chemistry Chemical Physics* **2016,** *18* (14), 9544-9553.
56. Lu, J.; Chakravarty, C.; Molinero, V., Relationship between the line of density anomaly and the lines of melting, crystallization, cavitation, and liquid spinodal in coarse-grained water models. *The Journal of Chemical Physics* **2016,** *144* (23), 234507.
57. Tersoff, J., New empirical approach for the structure and energy of covalent systems. *Physical Review B* **1988,** *37* (12), 6991-7000.
58. Gartner III, T. E.; Hunter, K. M.; Lambros, E.; Caruso, A.; Riera, M.; Medders, G. R.; Panagiotopoulos, A. Z.; Debenedetti, P. G.; Paesani, F., Anomalies and Local Structure of Liquid Water from Boiling to the Supercooled Regime as Predicted by the Many-Body MB-pol Model. *The Journal of Physical Chemistry Letters* **2022,** *13* (16), 3652-3658.
59. Poole, P. H.; Sciortino, F.; Essmann, U.; Stanley, H. E., Phase behaviour of metastable water. *Nature* **1992,** *360* (6402), 324-328.
60. Palmer, J. C.; Martelli, F.; Liu, Y.; Car, R.; Panagiotopoulos, A. Z.; Debenedetti, P. G., Metastable liquid–liquid transition in a molecular model of water. *Nature* **2014,** *510* (7505), 385-388.

61. Debenedetti, P., G.; Sciortino, F.; Zerze, G., H., Second critical point in two realistic models of water. *Science* **2020,** *369* (6501), 289-292.
62. Debenedetti, P. G.; Stanley, H. E., Supercooled and Glassy Water. *Physics Today* **2003,** *56* (6), 40-46.
63. Kim, K. H.; Späh, A.; Pathak, H.; Perakis, F.; Mariedahl, D.; Amann-Winkel, K.; Sellberg, J. A.; Lee, J. H.; Kim, S.; Park, J.; et al, Maxima in the thermodynamic response and correlation functions of deeply supercooled water. *Science* **2017,** *358* (6370), 1589-1593.
64. Caupin, F.; Arvengas, A.; Davitt, K.; Azouzi, M. E. M.; Shmulovich, K. I.; Ramboz, C.; Sessoms, D. A.; Stroock, A. D., Exploring water and other liquids at negative pressure. *Journal of Physics: Condensed Matter* **2012,** *24* (28), 284110.
65. Pallares, G.; El Mekki Azouzi, M.; González, M. A.; Aragones, J. L.; Abascal, J. L. F.; Valeriani, C.; Caupin, F., Anomalies in bulk supercooled water at negative pressure. *Proceedings of the National Academy of Sciences* **2014,** *111* (22), 7936-7941.
66. Altabet, Y. E.; Singh, R. S.; Stillinger, F. H.; Debenedetti, P. G., Thermodynamic Anomalies in Stretched Water. *Langmuir* **2017,** *33* (42), 11771-11778.
67. Plimpton, S., Fast parallel algorithms for short-range molecular dynamics. *Journal of computational physics* **1995,** *117* (1), 1-19.
68. Ryckaert, J.-P.; Ciccotti, G.; Berendsen, H. J. C., Numerical integration of the cartesian equations of motion of a system with constraints: molecular dynamics of n-alkanes. *Journal of Computational Physics* **1977,** *23* (3), 327-341.
69. Hockney, R. W.; Eastwood, J. W., Computer Simulation Using Particles (1st ed.). *CRC Press* **1988**.
70. Martínez, J. M.; Martínez, L., Packing optimization for automated generation of complex system's initial configurations for molecular dynamics and docking. *Journal of Computational Chemistry* **2003,** *24* (7), 819-825.
71. Matsumoto, M.; Yagasaki, T.; Tanaka, H., GenIce: Hydrogen-Disordered Ice Generator. *Journal of Computational Chemistry* **2018,** *39* (1), 61-64.
72. Humphrey, W.; Dalke, A.; Schulten, K., VMD: visual molecular dynamics. *Journal of molecular graphics* **1996,** *14* (1), 33-38.
73. Sedlmeier, F.; Horinek, D.; Netz, R. R., Spatial Correlations of Density and Structural Fluctuations in Liquid Water: A Comparative Simulation Study. *Journal of the American Chemical Society* **2011,** *133* (5), 1391-1398.
74. Nguyen, A. H.; Molinero, V., Identification of Clathrate Hydrates, Hexagonal Ice, Cubic Ice, and Liquid Water in Simulations: the CHILL+ Algorithm. *The Journal of Physical Chemistry B* **2015,** *119* (29), 9369-9376.
75. Moore, E. B.; de la Llave, E.; Welke, K.; Scherlis, D. A.; Molinero, V., Freezing, melting and structure of ice in a hydrophilic nanopore. *Physical Chemistry Chemical Physics* **2010,** *12* (16), 4124-4134.
76. Skinner, L. B.; Huang, C.; Schlesinger, D.; Pettersson, L. G. M.; Nilsson, A.; Benmore, C. J., Benchmark oxygen-oxygen pair-distribution function of ambient water from x-ray diffraction measurements with a wide Q-range. *The Journal of Chemical Physics* **2013,** *138* (7), 074506.
77. Skinner, L. B.; Benmore, C. J.; Neuefeind, J. C.; Parise, J. B., The structure of water around the compressibility minimum. *The Journal of Chemical Physics* **2014,** *141* (21), 214507.
78. Benmore, C.; Gallington, L. C.; Soignard, E., Intermediate range order in supercooled water. *Molecular Physics* **2019,** *117* (18), 2470-2476.
79. Pathak, H.; Späh, A.; Kim, K. H.; Tsironi, I.; Mariedahl, D.; Blanco, M.; Huotari, S.; Honkimäki, V.; Nilsson, A., Intermediate range O–O correlations in supercooled water down to 235 K. *The Journal of Chemical Physics* **2019,** *150* (22), 224506.
80. Hestand, N. J.; Skinner, J. L., Perspective: Crossing the Widom line in no man's land: Experiments, simulations, and the location of the liquid-liquid critical point in supercooled water. *The Journal of Chemical Physics* **2018,** *149* (14), 140901.
81. Chiu, J.; Starr, F. W.; Giovambattista, N., Heating-induced glass-glass and glass-liquid transformations in computer simulations of water. *The Journal of Chemical Physics* **2014,** *140* (11), 114504.
82. Chiu, J.; Starr, F. W.; Giovambattista, N., Pressure-induced transformations in computer simulations of glassy water. *The Journal of Chemical Physics* **2013,** *139* (18), 184504.
83. Wong, J.; Jahn, D. A.; Giovambattista, N., Pressure-induced transformations in glassy water: A computer simulation study using the TIP4P/2005 model. *The Journal of Chemical Physics* **2015,** *143* (7), 074501.
84. Finney, J. L.; Hallbrucker, A.; Kohl, I.; Soper, A. K.; Bowron, D. T., Structures of High and Low Density Amorphous Ice by Neutron Diffraction. *Physical Review Letters* **2002,** *88* (22), 225503.
85. Blazquez, S.; Vega, C., Melting points of water models: Current situation. *The Journal of Chemical Physics* **2022,** *156* (21), 216101.
86. García Fernández, R.; Abascal, J. L.; Vega, C., The melting point of ice I h for common water models calculated from direct coexistence of the solid-liquid interface. *The Journal of chemical physics* **2006,** *124* (14), 144506.
87. Nada, H., Anisotropy in geometrically rough structure of ice prismatic plane interface during growth: Development of a modified six-site model of H2O and a molecular dynamics simulation. *The Journal of Chemical Physics* **2016,** *145* (24), 244706.
88. Mishima, O., Relationship between melting and amorphization of ice. *Nature* **1996,** *384* (6609), 546-549.
89. Mishima, O., Melting of the Precipitated Ice IV in LiCl Aqueous Solution and Polyamorphism of Water. *The Journal of Physical Chemistry B* **2011,** *115* (48), 14064-14067.
90. Marion, G. M.; Jakubowski, S. D., The compressibility of ice to 2.0 kbar. *Cold Regions Science and Technology* **2004,** *38* (2), 211-218.
91. Bridgman, P. W., Water, in the Liquid and Five Solid Forms, under Pressure. *Proc. of the Am. Acad. of Art. and Sci.* **1912,** *47*, 441-558.
92. Anisimov, M. A.; Duška, M.; Caupin, F.; Amrhein, L. E.; Rosenbaum, A.; Sadus, R. J., Thermodynamics of fluid polyamorphism. *Physical Review X* **2018,** *8* (1), 011004.
93. Caupin, F.; Anisimov, M. A., Thermodynamics of supercooled and stretched water: Unifying two-structure description and liquid-vapor spinodal. *The Journal of Chemical Physics* **2019,** *151* (3), 034503.
94. Kanno, H.; Speedy, R. J.; Angell, C. A., Supercooling of Water to -92°C Under Pressure. *Science* **1975,** *189* (4206), 880-881.
95. Caupin, F.; Stroock, A. D., The Stability Limit and other Open Questions on Water at Negative Pressure. In *Liquid Polymorphism*, 2013; pp 51-80.
96. Qiu, C.; Krüger, Y.; Wilke, M.; Marti, D.; Rička, J.; Frenz, M., Exploration of the phase diagram of liquid water in the low-temperature metastable region using synthetic fluid inclusions. *Physical Chemistry Chemical Physics* **2016,** *18* (40), 28227-28241.
97. Romano, F.; Russo, J.; Tanaka, H., Novel stable crystalline phase for the Stillinger-Weber potential. *Physical Review B* **2014,** *90* (1), 014204.
98. Zheng, Q.; Durben, D.; Wolf, G.; Angell, C., Liquids at large negative pressures: water at the homogeneous nucleation limit. *Science* **1991,** *254* (5033), 829-832.
99. Pallares, G.; Gonzalez, M. A.; Abascal, J. L. F.; Valeriani, C.; Caupin, F., Equation of state for water and its line of density

maxima down to− 120 MPa. *Physical Chemistry Chemical Physics* **2016,** *18* (8), 5896-5900.
100. Conde, M. M.; Vega, C.; Tribello, G. A.; Slater, B., The phase diagram of water at negative pressures: Virtual ices. *The Journal of Chemical Physics* **2009,** *131* (3), 034510.
101. Bianco, V.; de Hijes, P. M.; Lamas, C. P.; Sanz, E.; Vega, C., Anomalous Behavior in the Nucleation of Ice at Negative Pressures. *Physical Review Letters* **2021,** *126* (1), 015704.
102. Bertolazzo, A. A.; Kumar, A.; Chakravarty, C.; Molinero, V., Water-like Anomalies and Phase Behavior of a Pair Potential that Stabilizes Diamond. *The Journal of Physical Chemistry B* **2016,** *120* (8), 1649-1659.

TOC Graphic